Journal of Advanced Marine Engineering and Technology, Vol. 47, No. 6, pp. 285~294, 2023
J. Advanced Marine Engineering and Technology (JAMET)
https://doi.org/10.5916/jamet.2023.47.6.285

ISSN 2234-7925 (Print)
ISSN 2765-4796 (Online)
Original Paper

Effects of reaction temperature and residence time on the thermal decomposition of N_2O in thermal reactor

Suhyeon Kim[1] · Dae Geun Park[2] · Seung Gon Kim[3] · Sung Hwan Yoon[†]

(Received November 27, 2023 ; Revised December 1, 2023 ; Accepted December 20, 2023)

Abstract: Global response efforts to global warming are required, and in particular, countries affiliated with the Paris Agreement have set and implemented voluntary reduction targets to reduce greenhouse gas emissions. Nitrous oxide (N_2O), a greenhouse gas, is known to be a major chemical species in the depletion of the ozone layer, with a global warming potential (GWP) 310 times greater than that of CO_2 and a decomposition period of 120 years. This study adopted a high-temperature pyrolysis method to decompose N_2O and conducted numerical and experimental studies simultaneously. In particular, it focused on the correlation between N_2O reduction and NOx and N_2 formation. Consequently, the N_2O decomposition rate increased as the reaction temperature increased, and almost all of the N_2O was converted into N_2 at a reaction temperature of 1400 K. Most of the NOx generated was converted to NO and some NOx was converted to NO_2. The effect of the residence time on N_2O in the high-temperature region was observed only at reaction temperatures below 1400 K, and this was not confirmed because of the chemical equilibrium state at 1400 K or higher.

Keywords: Nitrous oxide (N_2O), Nitric oxide (NOx), Greenhouse gas, High-temperature pyrolysis

1. Introduction

Greenhouse gases contribute to global warming. The Kyoto Protocol, adopted at the Third Conference of the Parties (COP 3) of the United Nations Framework Convention on Climate Change (UNFCCC), designates six greenhouse gases—carbon dioxide (CO_2), methane (CH_4), nitrous oxide (N_2O), hydrofluorocarbons (HFCs), perfluorocarbons (PFCs), and sulfur hexafluoride (SF_6)—as targets for reduction **[1]**.

N_2O, the third highest emitter among greenhouse gases, has a global warming potential (GWP) that is more than 300 times higher than that of CO_2 and has remained in the atmosphere for more than 120 years with a chemically stable structure **[2]**. Additional details on this can be found in **Table 1**. N_2O reaches the stratosphere and reacts with ozone, and the ozone depletion process proceeds according to the following reaction mechanism **[3]**.

$$2N_2O \rightarrow 2N_2 + O_2 \quad (1)$$

$$O_3 \leftrightarrow O_2 + O \quad (2)$$

$$N_2O + O \rightarrow 2NO \quad (3)$$

$$NO + O_3 \rightarrow NO_2 + O_2 \quad (4)$$

$$NO_2 + O \rightarrow NO + O_2 \quad (5)$$

Greenhouse gases interfere with the global infrared energy, which must be emitted for the energy balance of the earth, and change the global environment in various fields such as ecosystems, food, and natural disasters **[4]**.

According to the 5th Climate Assessment Report in 2014 of UN Intergovernmental Panel on Climate Change (UN IPCC), global greenhouse gas emissions must be reduced by up to 70 % by 2050 compared with 2010 to maintain the average global temperature rise below 2 °C **[5]**. In addition, the Paris Agreement adopted by COP 21 in 2015 proposed that Nationally Determined Contributions (NDCs) should be regulated and observed in each country **[6]**.

† Corresponding Author (ORCID: https://orcid.org/0000-0001-5794-3286): Associate Professor, Department of Marine System Engineering, Korea Maritime & Ocean University, 727, Taejong-ro, Yeongdo-gu, Busan 49112, Korea, E-mail: shy@kmou.ac.kr, Tel: +82-51-410-4261

1 M. S. candidate, Department of Marine System Engineering, Korea Maritime & Ocean University, E-mail: edwsqsa8624@g.kmou.ac.kr, Tel: +82-51-410-4261

2 Principle researcher, Carbon Neutral Technology R&D Department, Korea Institute of Industrial Technology, E-mail: dgpark@kitech.re.kr

3 Principle researcher, Energy Efficiency Research Division, Korea Institute of Energy Research, E-mail: kimsg@kier.re.kr

In accordance with the Paris Agreement and Kyoto Protocol, greenhouse gas reduction targets to be implemented in the shipping industry have been delegated to the International Maritime Organization (IMO) **[8]**. In September 1997, the International Convention for the Prevention of Marine Pollution from Ships (MARPOL) Annex VI was established to regulate CO_2 emissions **[9]**. Additionally, during the 72nd Marine Environmental Protection Committee (MEPC 72), the IMO's initial GHG strategy for greenhouse gas reduction in shipping was adopted, aiming at a 50 % reduction by 2050 compared with 2008 levels **[10]**. The revised GHG strategy in 2023 further elevates the goal of achieving net zero emissions by 2050 **[11]**.

Shipping companies are adopting carbon alternative fuels in response to greenhouse gas regulations **[8]**. Ammonia, methanol, hydrogen, LNG, and LPG are among the carbon alternative fuels used. Among these, ammonia is the most prominent, and the International Energy Agency (IEA) forecasts that by 2050, ammonia will account for nearly half of the fuels consumed by the shipping industry **[12]**. Ammonia has a vapor pressure of 1.46 MPa at 37.8 °C, enabling relatively easy liquefaction. It is lighter than air, facilitating good ventilation, and its tendency to disperse at higher elevations allows for effective control of leaked gases. Additionally, ammonia, similar to hydrogen, does not contain carbon, and its ability to remain in a liquid state under approximately 1 MPa pressure at ordinary temperature allows for the continued use of the existing LPG infrastructure **[8]**. However, owing to the oxidation of ammonia, N_2O emissions are expected to increase **[13][14]**.

Moreover, most of the causes of N_2O emissions are the result of human economic and industrial activities such as semiconductor processes and adipic acid and nitric acid production facilities. The semiconductor process that generates N_2O consists of eight processes; N_2O is used as an oxidizer when an insulating film is formed on an Si substrate by the CVD method used in the oxidation process **[15]**. In the manufacturing process of adipic acid, N_2O that is generated when a mixture of cyclohexanol and cyclohexanone or only cyclohexanone reacts with N_2 to synthesize adipic acid accounts for 7−50 % of the emissions **[16]**.

N_2O treatment technology is divided into concentration and recovery, catalytic decomposition, and thermal decomposition treatments according to the physical method **[17]**. Concentration and recovery are efficient methods; however, they have the disadvantage of high maintenance costs. Catalytic decomposition can be divided into selective catalytic reduction, selective non-catalytic reduction, and direct catalytic reduction **[18]**. Selective non-catalytic reduction and selective catalytic reduction have high processing efficiency but require difficult operation technology or high maintenance costs. Direct catalytic reduction has advantages in efficiency and maintenance cost because the reductant is not used; however, it has the disadvantage of high uncertainty because it has never been demonstrated in commercial processes **[19]**. Although the thermal decomposition treatment method has significant advantages in terms of operation owing to its low technical difficulty, it has the disadvantage of increasing NOx emissions.

In previous studies on N_2O reduction, Jo *et al.* reported that the reduction efficiency of N_2O increased when O_2 content was small or plasma was applied **[20]**. Park *et al.* reported that most of the N_2O thermally decomposed under high-temperature conditions was converted to N_2 and that a higher reaction temperature and longer residence time resulted in a higher reduction rate of N_2O **[21]**. Jin *et al.* reported that a flow structure in a vortex form was formed by a K−H instability according to the nozzle exit velocity, and in the result, the residence time of N_2O for surrounding flow increased and emissions of NO_2 significantly reduced **[22]**. An *et al.* reported that the reduction in NOx increased as the residence time of gases in the catalyst layer increased **[23]**. Lee *et al.* conducted studies on N_2O decomposition and NOx formation in a high-temperature reactor and experimentally confirmed that N_2O reduction efficiency

Table 1: Global warming potential of greenhouse gases in Reference **[7]**

Greenhouse Gas, GHG	Global Warming Potential			Lifetimes [years]
	20 years	100 years	500 years	
CO_2	1	1	1	Variable
CH_4	56	21	6.5	9–15
N_2O	280	310	170	120
HFCs	460–6,100	140–11,700	42–9,800	1.5–264
SF_6	16,300	23,900	34,900	3,200
PFCs	4,400–6,200	6,500–9,200	10,000–14,000	2,600–50,000

prevailed under specific operating conditions, depending on the reaction temperature and residence time **[24]**. However, Lee *et al*. conducted experiments using relatively low concentrations of N_2O in an argon atmosphere; this was difficult to apply to the actual high-temperature thermal decomposition process using air as an oxidizer.

Therefore, in this experiment, the same air as the actual industrial environment was adopted as the atmospheric gas, and a high concentration N_2O of 100,000 ppm or more was supplied to the high-temperature reactor to apply to the semiconductor process. Furthermore, we compared the experimental results with the numerical results calculated using CHEMKIN−PRO to establish the interaction of N_2O reduction and NOx formation mechanisms in thermal decomposition treatment.

2. Experimental and Numerical Methods

2.1 Experimental method

Figure 1 shows a schematic diagram of the high-temperature reactor and measuring equipment used to estimate the thermal decomposition characteristics of N_2O. The experimental setup comprised a high-temperature reactor, flow control part, measurement part, and an exhaust port.

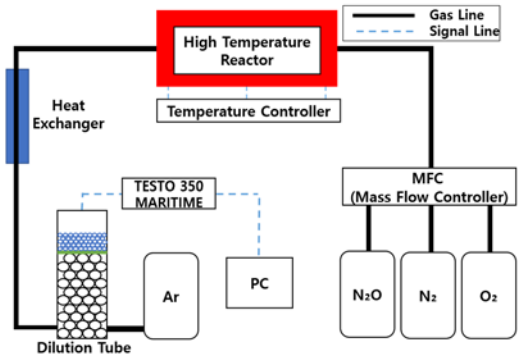

Figure 1: Schematic diagram of the experimental setup

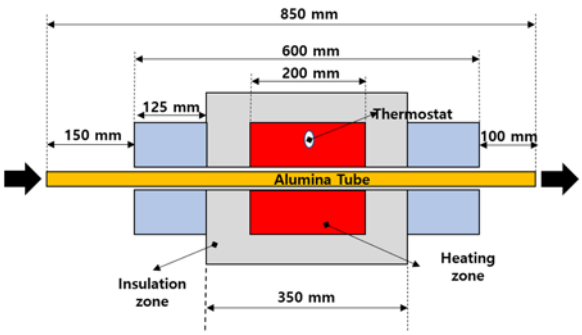

Figure 2: Inner structure of the reactor

Figure 2 shows the internal structure of the high-temperature reactor consisting of a cylindrical alumina tube with a length of 850 mm and an inner diameter of 10 mm. In the 200 mm section at the center part of the reactor, a high temperature was uniformly supplied to the inside of the reactor through six heating coils installed around the outer surface of the tube. The supplied heat was measured using R-type thermocouples installed inside and outside the tube, and the maximum saturation temperature at the center of the tube was set to the reaction temperature. **Figure 3** shows the internal temperature distribution of the alumina tubes with various amounts of heat supplied according to the length direction. As shown in **Figure 3**, the internal temperature was saturated at a constant temperature in the 350–550 mm section corresponding to the central part of the reactor in all measured cases. The reactor interior was configured as an insulation zone to shield the internal temperature from external influences.

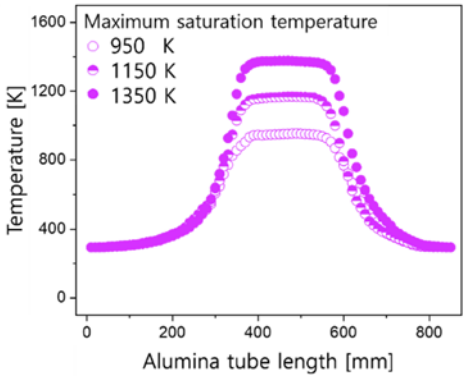

Figure 3: Internal temperature distribution in the alumina tube with various amounts of heat supplied

The gas composition used in the experiment was selected as single gas composition of 71.1 % N_2, 18.9 % O_2, and 100,000 ppm N_2O to simulate the actual industrial environment. The selected gas was supplied to the reactor through mass flow controllers (MFCs) corrected using a gas calibrator (MesaLabs, Defender 530+H). The injected gas was discharged after thermal decomposition. The discharged gas was cooled using a heat exchanger and measured using a combustion gas analysis system for ships (TESTO 350 MARITIME). The measurable range of NOx in the combustion gas analysis system for ships is approximately 500 ppm for NO_2 and approximately 3,000 ppm for NO. However, the concentration of NOx discharged in the present experiment was expected to fall outside this range; the discharged gas was diluted with a dilution gas in a dilution tube for gas concentration analysis. Argon, that has low reactivity

even at high temperatures was used as the dilution gas. In the dilution tube, the ceramic bid and mesh were installed together to ensure uniform gas flow and remove moisture through silica gel. In the experimental method, the gas concentration was measured for 1 min after 3 min after the reactor internal temperature reached the target, and the external temperature and pressure were maintained at 25 °C and 1 atm, respectively.

The experimental variables were selected by reaction temperature and residence time, and the details are listed in **Table 2**. In a previous study, the decomposition of N_2O began in the range of 1000–1100 K **[25]**, and the emission of NOx increased as the reaction temperature increased. To validate these characteristics, we selected reaction temperatures ranging from 1100 to 1500 K. Additionally, considering previous research results indicating a decrease in NOx at lower temperatures for the same residence time, we selected residence time as a variable because the emission of NOx varied with changes in residence time **[26]**.

Table 2: Experimental conditions

Conditions	Values
Temperature [K]	1100, 1200, 1300, 1400, 1500
Residence time [s]	1, 2, 4

The mixed flow rate corresponding to each residence time is as follows:

$$Q = \frac{\pi \times (\frac{D}{2})^2 \times L}{t} \quad (6)$$

Here, Q is the gas mixture flow rate, D is the inner diameter of the reactor, L is the length of the reactor, and t is the residence time.

To compensate for the gas expansion rate owing to the reaction temperature, the volumetric flow rate of the gas mixture was controlled using Charles' law.

$$\frac{Q_1}{T_1} = \frac{Q_2}{T_2} \quad (7)$$

Here, Q_1 is the inlet flow rate, T_1 is the inlet temperature, Q_2 is the flow rate at each value of residence time, and T_2 is the reactor temperature.

2.2 Numerical Method

A numerical analysis was performed using a plug flow reactor, a one-dimensional reaction structure analysis model based on CHEMKIN **[27]**. The plug flow reactor can set the inner diameter, length, pyrolysis temperature, injected gas, and flow velocity, and information on the products produced after the thermal decomposition of the selected gas can be obtained. The calculation conditions in this study adopted the same diameter, residence time, and reaction temperature as in the experimental conditions, and the tube length was set to 200 mm that corresponded to the maximum saturation temperature range, as shown in **Figure 3**. We calculated the N_2O chemical reaction using GRI 3.0 mechanism that is widely used for modeling NO generation and reburn chemistry **[28]**. As presented in **Table 3**, the rate of each reaction was evaluated using a reaction path analyzer.

3. Results and Discussion

3.1 Numerical Analysis Results

3.3.1 Overall trend of N_2O Decomposition by High-Temperature Pyrolysis

Figure 4 shows the variations in the concentrations of N_2O (**Figure 4(a)**), NO_2, NO, and N_2 (**Figure 4(b)**) according to various reaction temperatures at t_{reac} = 1 s. The initial supply of N_2O is 100,000 ppm. The concentration of N_2 is considered only as the concentration, excluding the initial supply from the measured amount. The N_2O concentration is linearly reduced at T_{reac} = 1100−1300 K, and 20.6 ppm and 0.19 ppm are derived at

Table 3: GRI 3.0 mechanism

Reaction	(k=AT^{b}exp(-E/RT)		
	A	b	E
$N_2O+M \Leftrightarrow N_2+O+M$	7.9E+10	0	56020
$N_2O+O \Leftrightarrow N_2+O$	1.4E+12	0	10810
$N_2O+O \Leftrightarrow 2NO$	2.9E+13	0	23150
$NO_2+O \Leftrightarrow NO+O_2$	3.9E+12	0	-240
$NO+O+M \Leftrightarrow NO_2+M$	1.0E+20	-1.41	0
$N+NO \Leftrightarrow N_2+O$	2.7E+13	0	355
$N+O_2 \Leftrightarrow NO+O$	9.0E+09	1	6500

T_{reac} = 1400 K and 1500 K, respectively, indicating that almost all N_2O is decomposed. In the case of the NO_2 concentration, as illustrated in **Figure 4(b)**, as the reaction temperature increases, the NO_2 concentration increases linearly from 1100 K to 1300 K, and approximately 100 ppm is generated from 1300 K and the amount of production is saturated. The N_2 concentration also is generated 6.0 × 10^4 ppm at T_{reac} = 1300 K, and the amount of production is saturated. However, in the case of NO concentration, the amount of production increases linearly as the reaction temperature increases, and 1.9 × 10^4 ppm, the maximum concentration value, is generated at T_{reac} = 1500 K.

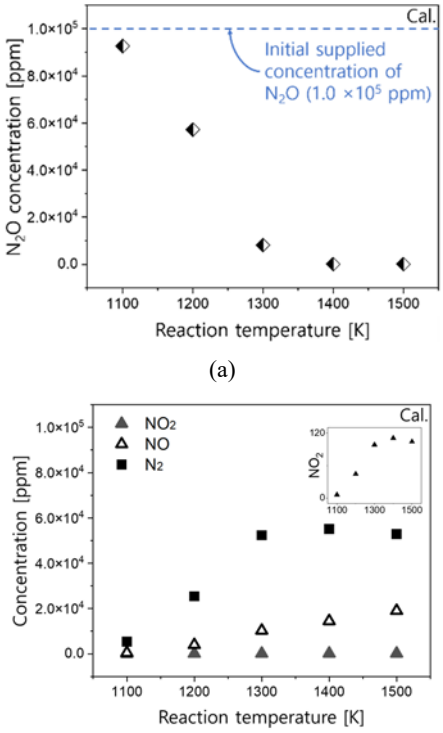

Figure 4: Concentrations of gas species according to various reaction temperatures at t_{reac} = 1 s; (a) N_2O, (b) NO_2, NO, and N_2

Generally, according to the Zel'dovich mechanism **[28]**, N_2O decomposes into N and O at high temperatures, and the decomposed O and N_2O react to produce N_2 and O_2. At this time, NO and NO_2 are partially generated according to **Equations (10)** and **(11)**, and the general reaction mechanism is as follows:

$$N_2O \rightarrow N_2 + O \quad (8)$$

$$N_2O + O \rightarrow N_2 + O_2 \quad (9)$$

$$N_2O + O \rightarrow 2NO \quad (10)$$

$$NO + O \rightarrow NO_2 \quad (11)$$

In addition, most of the N_2O injected at a reaction temperature of 1300 K is decomposed, and the formation rates of NO_2 and N_2 are saturated. However, the rate of NO production increases with increasing reaction temperature. To understand this more clearly, Section 3.1.2 provides the correlation between N_2O reduction and NOx and N_2 production according to reaction temperatures and residence times.

3.3.2 Correlation between N_2O Reduction and NOx and N_2 Production according to Reaction Temperatures and Residence times

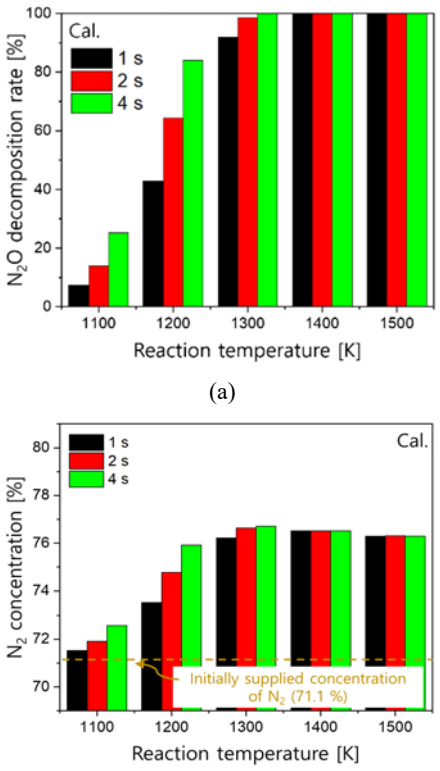

Figure 5: (a) N_2O decomposition rates and (b) N_2 concentrations with various reaction temperatures and residence times

Figure 5 shows the N_2O decomposition rates and N_2 concentrations at various reaction temperatures and residence times. The N_2O decomposition rate is calculated using **Equation (12)**.

$$N_2O \text{ reduction } (\%) = \frac{\text{Reduced } N_2O \text{ concentration}}{\text{Inlet } N_2O \text{ concentration}} \quad (12)$$

As shown in **Figure 5(a)**, the N_2O reduction rate increases for T_{reac} = 1100–1300 K as the residence time increases at the same reaction temperature. However, the N_2O reduction rate is not linearly proportional to the residence time. In addition, the N_2O reduction rate tends to reach 100 % for all the residence times adopted at T_{reac} = 1400 K. In the case of N_2 concentration, as shown in **Figure 5(b)**, considering that the initial supply concentration is 71.1 %, the trend in the N_2O reduction rate is similar. Therefore, the saturation temperature is close to 1400 K because the same N_2 concentration is considered irrespective of the residence time at T_{reac} = 1400 K. Particularly, at t_{reac} = 2 and 4 s, the N_2 concentration decreases slightly after T_{reac} = 1300 K, and the tendency to decrease after T_{reac} = 1400 K is observed at t_{reac} = 1 s.

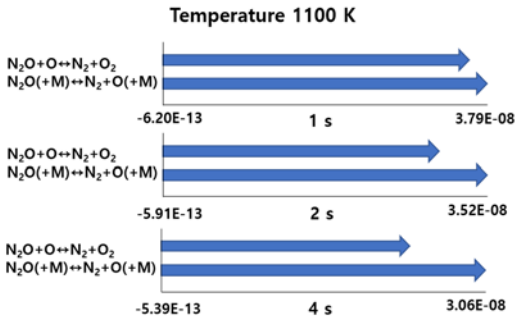

(a)

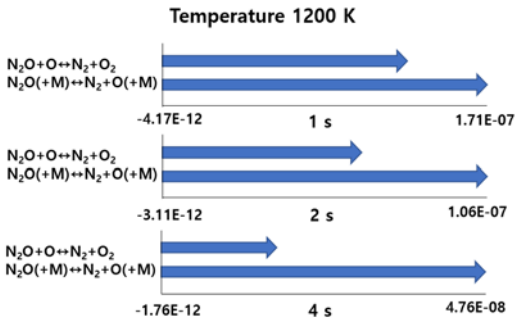

(b)

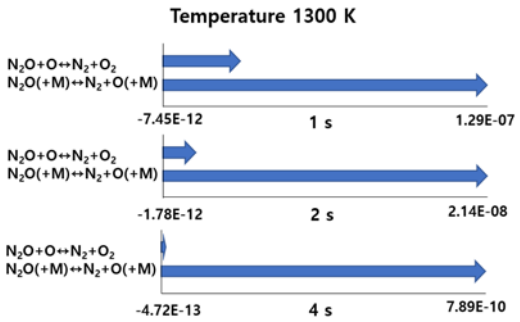

(c)

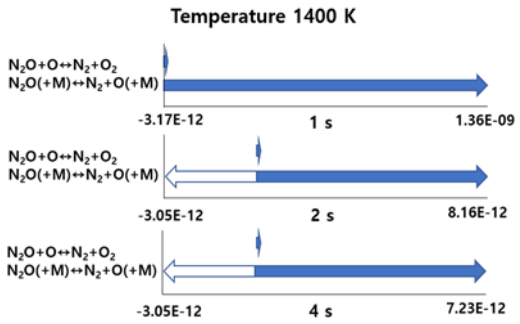

(d)

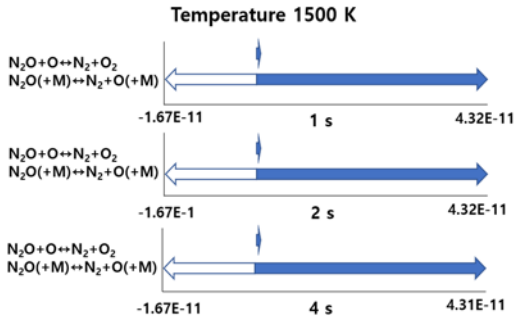

(e)

Figure 6: Rate of progress from N_2O to N_2

To clarify these aspects, **Figure 6** illustrates the reaction path analyzer for the rate of progress from N_2O to N_2 under the same conditions as in **Figure 5**. In the range of T_{reac} = 1100–1300 K, the reaction progress rate tends to decrease as the residence time increases. The chemical reaction rate is affected by the total amount of reactants injected per unit time, and the residence time is relatively longer than the reaction time. Therefore, the final N_2O concentration decreases; however, the volume of N_2O decomposed per unit time decreases. Finally, the reduction rate of N_2O is not linearly proportional to the residence time at the same reaction temperature (T_{reac} = 1100–1300 K), as shown in **Figure 5(a),** because of the decrease in the most dominant reaction progression from N_2O to N_2 (**Equations (8)** and **(9)**) during N_2O decomposition.

Meanwhile, after T_{reac} = 1400 K and t_{reac} = 2 s, the reverse reaction increases noticeably, as shown in **Figure 6(d)**. Notably, the reaction rate up to 1400 K and 1 s increases with increasing reaction temperature and residence time, whereas the forward reaction rate decreases significantly. This tendency is considered to have reached the chemical equilibrium state, considering that both the forward and reverse reaction rates are obtained at a constant value irrespective of the residence time at T_{reac} = 1500 K. Therefore, it is understood that the rapid increase in the reverse reaction from N_2O to N_2 causes the slight decrease in the

concentration of N_2 formation in the range of T_{reac} = 1400–1500 K, as shown in in **Figure 5(b)**. Furthermore, because the decomposition reaction from N_2O to N_2 reached a chemical equilibrium state at T_{reac} = 1500 K, the N_2O decomposition rate is expected to saturate after T_{reac} = 1500 K.

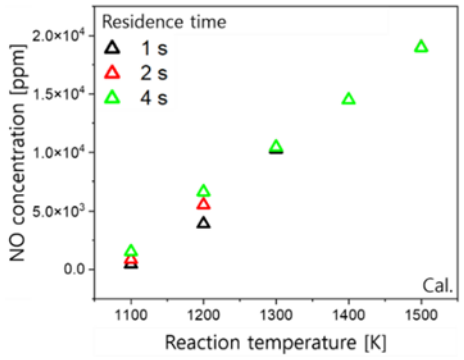

(a)

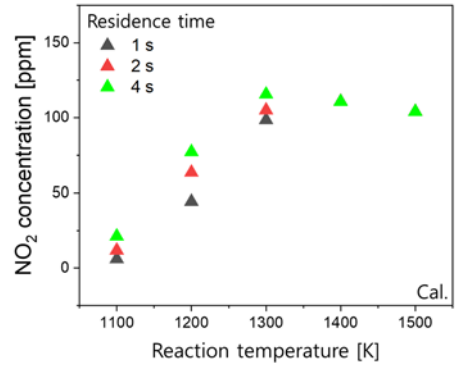

(b)

Figure 7: NO and NO_2 concentrations with various reaction temperatures and residence times

Figure 7 shows the formation concentrations of NO and NO_2 according to the reaction temperature and residence time. The formation concentrations of NO and NO_2 are not highly dependent on the residence time, and are independent of the residence time adopted in this study, after T_{reac} = 1400 K. However, as shown in **Figure 4(b)**, the formation concentration of NO increased linearly with the reaction temperature; this differed from the concentration trends of NO_2 and N_2. This is not easily understood, considering that, as shown in **Figure 4(a)**, the concentration of N_2O is typically decomposed and saturated at T_{reac} = 1300 K. In other words, chemical species other than N_2O exist that contribute to the formation of NO at T_{reac} = 1300 K or higher.

To investigate this aspect, **Figure 8** illustrates the absolute production rate (forward reaction rate-reverse reaction rate) with conversions of (a) NO_2–NO and (b) N–NO according to various reaction temperatures at t_{reac} = 1 s. In the case of NO_2–NO conversion, the $NO_2+O \rightarrow NO+O_2$ and $NO+O+M \rightarrow NO_2+M$ reactions are dominated. However, as shown in **Figure 8(a)**, oxidized reaction from NO to NO_2 are superior in both reactions.

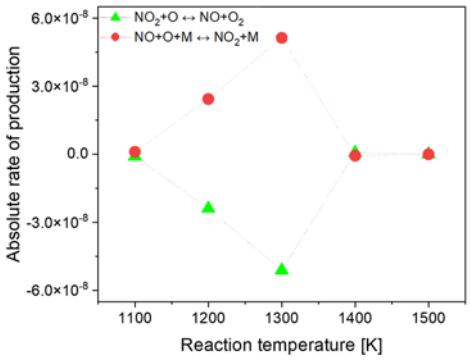

(a)

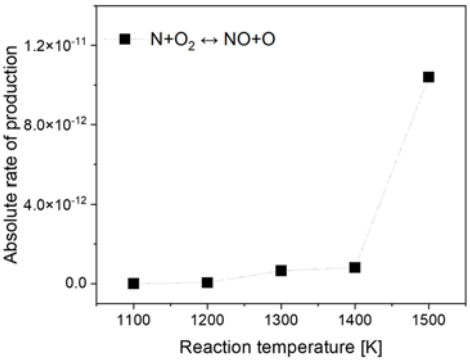

(b)

Figure 8: Absolute rate of production of conversion between (a) NO_2–NO and (b) N–NO

Therefore, the conversion of NO_2–NO does not contribute to the production of NO. In the case of N–NO conversion, the $N+O_2 \rightarrow NO+O$ reaction is dominated. However, as shown in **Figure 8(b)**, the absolute production rate has a positive value at all reaction temperatures, particularly, the process of oxidation from N to NO at T_{reac} = 1500 K increases sharply. Thus, N contributes to NO production via high-temperature reactions. This analogy is reasonable considering the results shown in **Figure 5(b)**.

3.2 Experimental Verification

In this section, the calculation results derived thus far are compared with the experimental results using a high-temperature reactor. **Figure 9** shows the results of comparing NO and NO_2 concentrations according to various reaction temperatures and residence times with the experimental and calculated values. The calculated values are derived from **Figures 7(a)** and **(b)**, and the

dependence on the residence time is extremely small; therefore, they are displayed as single dotted lines. In the case of NO concentration, both the experimental and numerical values show little dependence on the residence time. In addition, the tendency of linear increase is the same depending on the reaction temperature. However, the calculated value of the formation concentration is approximately 19,000 ppm, whereas the experimental value is approximately 7,000 ppm; the difference is approximately three times. For the NO_2 concentration, the calculated value is as shown in **Figure 7(b)**, and the dependence on the residence time is minimal and saturated at T_{reac} = 1400 K. However, the experimental value shows that the concentration of NO_2 formation increases rapidly as the residence time is shortened.

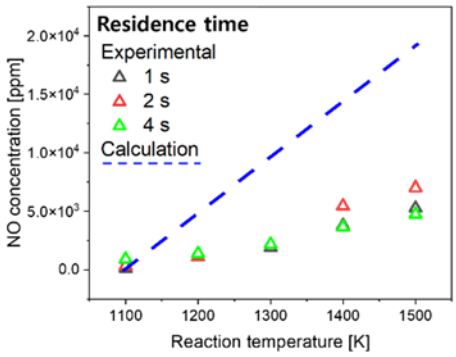

(a)

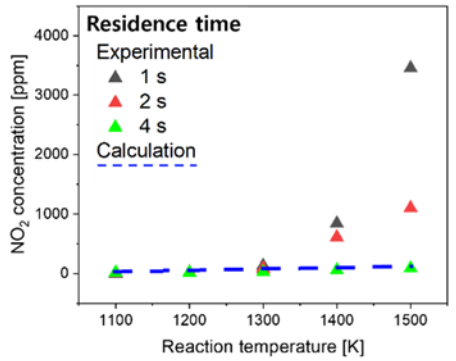

(b)

Figure 9: Concentrations of experimental and calculated results obtained for (a) NO and (b) NO_2

Furthermore, the concentration of NO_2 formation increases exponentially as the reaction temperature increases. In particular, the NO_2 concentrations of the experimental and calculated values match well in the case of t_{reac} = 4 s; however, a large difference is observed in the cases of t_{reac} = 1 and 2 s. Particularly, at t_{reac} = 1 s and T_{reac} = 1500 K, the calculated value of the concentration of NO_2 formation is approximately 100 ppm, whereas the maximum value of approximately 3400 ppm is measured in the experiment.

The experimental results are as follows: The dependence of the NO formation concentration on the residence time is determined to be derived at a constant value because the conversion from N_2O to NO is rapid within the selected residence time and all reach saturation under the present experimental conditions. This is the same with the calculated value. Therefore, to evaluate the dependence on the residence time, the experiment must be conducted within a shorter time than the present experimental conditions. In addition, the difference in the maximum NO concentration occurs because the gas discharged after the reaction was cooled through a heat exchanger for concentration analysis and diluted with a dilution gas in the dilution tube in the experiment; however, the reactor was set by insulation conditions in the numerical analysis. Therefore, a reverse reaction is generated, in which NO in a high-temperature state is converted to NO_2 by cooling.

As mentioned in Section 3.3.2, the reactions related to NO_2–NO conversion include $NO_2+O \rightarrow NO+O_2$ and $NO+O+M \rightarrow NO_2+M$, and temperature dependent constant “b” for these reactions are 0 and -1.41, respectively. The temperature dependent constant of -1.41 for reaction $NO+O+M \rightarrow NO_2+M$ indicates that as the reaction temperature increases, the rate constant increase for this reaction decreases. In the experiments, after passing through the central part of the reactor where the coils are installed, the temperature decreases. As a result, the $NO+O+M \rightarrow NO_2+M$ reaction increases again. With an increase in the reaction temperature, the production of NO increases, leading to an increase in the amount of NO that can be converted to NO_2.

Consequently, the experimental results show a tendency of increasing NO_2 emissions with increasing reaction temperature. However, the numerical analysis focuses only on the reactions in the middle part of the reactor where the coils are installed. Thus, it could not accurately predict the production of NO_2.

4. Conclusion

This study investigated the interaction between N_2O reduction and NO generation mechanisms in a high-temperature pyrolysis treatment using a one-dimensional reaction structure analysis model. Comparative verification was performed with the experimental values obtained in a high-temperature reactor. The

reaction temperature and residence time were selected as evaluation factors. A GRI 3.0 mechanism was adopted to characterize the correlation between N_2O reduction and NOx and N_2 formation. The calculation and experimental results are summarized as follows:

1. According to the calculation, as the reaction temperature increased, the decomposition rate of N_2O increased, and almost all of the N_2O injected at a reaction temperature of 1400 K decomposed to reach a chemical equilibrium state.
2. As N_2O decomposed, N_2, NO, and NO_2 were generated, and the formation rates of N_2 and NO_2 were saturated at a reaction temperature of 1400 K, similar to the tendency of the N_2O decomposition rate. However, in the case of the formation rate of NO, unlike the formation tendency of N_2 and NO_2, the formation rate continued to increase as the reaction temperature increased. Analyzing the progress rate using a reaction path analyzer to investigate these causes confirmed that the process of oxidation from N to NO increased rapidly as the reaction temperature increased, contributing to NO formation.
3. Notably, the formation concentrations of N_2, NO, and NO_2 were not largely dependent on the residence time, and particularly from the reaction temperature of 1400 K, they were independent of the residence time adopted in this study. This was because the reaction rate from N_2O to N_2, which is the most dominant N_2O decomposition reaction, was constantly obtained from a reaction temperature of 1400 K. Therefore, the chemical equilibrium was reached.
4. As a result of conducting a comparative analysis of the high-temperature reactor experimental results and the calculation results indicated that, in both cases, the NO formation concentration was obtained as a constant value depending on the residence time. In addition, the maximum NO formation concentration value obtained in the experiment was clearly different when compared to the calculated value. In the case of calculation, a reverse reaction occurred in which NO_2 was converted to NO owing to the process of cooling in the heat exchanger for concentration analysis. Similar results were obtained in the comparative analysis of the NO_2 concentration.

Acknowledgements

This work was supported by the Technology Innovation Program (20015606, Development of the POU Scrubber with Smart Control for Simultaneous Reduction of Greenhouse Gases and Fine Dusts emitted from the Semiconductor and Display Manufacturing Process) funded By the Ministry of Trade, Industry & Energy (MOTIE, Republic of Korea).

Author Contributions

Conceptualization, S. Kim and S. H. Yoon; Methodology, S. Kim and S. G. Kim; Software, S. Kim and S. G. Kim; Validation, S. Kim and S. H. Yoon; Formal Analysis, S. Kim and D. G. Park; Investigation, S. Kim and D. G. Park; Resources, S. Kim; Data Curation, S. Kim; Writing—Original Draft Preparation, S. Kim; Writing—Review & Editing, S. H. Yoon; Visualization, S. Kim; Supervision, S. H. Yoon; Project Administration, S. H. Yoon; Funding Acquisition, S. H. Yoon

References

[1] United Nations(UN), Kyoto Protocol to the United Nations Framework Convention on Climate Change, United Nations: Geneva, Switzerland, 1998.

[2] D. J. Griggs and M. Noguer, “Climate change 2001: The scientific basis. Contribution of working group I to the third assessment report of the intergovernmental panel on climate change,” Weather, vol. 57, no. 8, pp. 267-269, 2002.

[3] M. Campbell and J. M. Tom Pierce, “Atmospheric science, anaesthesia, and the environment,” BJA Education, vol. 15, no. 4, pp. 173-179, 2015.

[4] D. H. Shin, D. C. Lee, and J. G. Nam, “A study on the trend of recent research for the GHG reduction from ships,” 2008 Proceedings of the Korean Society of Marine Engineering, pp. 107-111, 2008 (in Korean).

[5] R. K. Pachauri, M. R. Allen, V. R. Barros, J. Broome, … and J. -P. van Ypserle, “Climate change 2014: Synthesis report. Contribution of working groups I, II and III to the fifth assessment report of the intergovernmental panel on climate change,” Geneva, Switzerland, The Intergovernmental Panel on Climate Change (IPCC), pp. 92-93, 2014.

[6] S. UNFCCC, “Report of the conference of the parties on its twenty-first session, held in Paris from 30 November to 13 December 2015, Addendum. Part two: Action taken by the conference of the parties at its twenty-first sess,” United Nations Framework Convention on Climate Change Bonn, vol. 3, 2015.

[7] IPCC, “Climate Change 1995: IPCC Second Assessment Report,” Intergovernmental Panel on Climate Change, 1995.

[8] Korean Register (KR), Ammonia-Fueled Propulsion Vessels Report, 2021.

[9] International Maritime Organization(IMO), Protocol of 1997 to Amend the International Convention for the Prevention of Pollution from Ships of 2 November 1973, as Modified by the Protocol of 17 February 197, London, 1997.

[10] IMO MEPC72, Initial IMO Strategy on Reduction of GHG Emissions from Ships, Resolution MEPC, vol. 304, 2018.

[11] IMO MEPC80. 2023 IMO Strategy on Reduction of GHG Emissions from Ships, Resolution MEPC, vol. 377, 2023.

[12] IEA, World Energy Outlook 2019, 2019.

[13] H. K. Lee, Y. M. Woo, and M. J. Lee, “The needs for R&D of Ammonia combustion technology for carbon neutrality-part II R&D trends and technical feasibility analysis,” Journal of The Korean Society of Combustion, vol. 26, no. 1, pp. 84-106, 2021.

[14] S. Hui, Q. Yao, D. Wang, and Y. Niu, “Effect of oxygen on N_2O and NO formation from NH_3 oxidation over MnO_x/TiO_2 catalysts,” Energy Procedia, vol. 158, pp. 1497-1501, 2019.

[15] J. H. Cho, T. H. Lee, and J. K. Park, “A study on the N_2O separation process from crude N_2O,” Korean Chemical Engineering Research, vol. 43, no. 4, pp. 467-473, 2005.

[16] E. V. Ovchinnikova, V. A. Chumachenko, L. V. Piryutko, A. C. Kharitonov, and A. S. Noskov, “Detoxication of nitrose gases formed in the production of adipic acid: The two-stage catalytic cleaning process,” Catalysis in Industry, vol. 1, pp. 76-84, 2009.

[17] K. S. Chang, “Status and trends of emission reduction technologies and CDM projects of greenhouse gas nitrous oxide,” Applied Chemistry for Engineering, vol. 19, no. 1, pp. 17-26, 2008 (in Korean).

[18] K. B. Nam and S. C. Hong, “N_2O decomposition characteristics and efficiency enhancement of Rh/CeO_2 catalyst,” Applied Chemistry for Engineering, vol. 29, no. 5, pp. 541-548, 2018.

[19] S. G. Lee, H. J. Lee, I. H. Song, S. H. Youn, D. H. Kim, and S. J. Cho, “Suppressed N_2O formation during NH_3 selective catalytic reduction using vanadium on zeolitic microporous TiO_2,” Scientific Reports, vol. 5, no. 1, pp. 12702, 2015.

[20] J. O. Jo, Q. H. Trinh, S. H. Kim, and Y. S. Mok, “Plasma-catalytic decomposition of nitrous oxide over γ-alumina-supported metal oxides,” Catalysis Today, vol. 310, pp. 42-48, 2018.

[21] J. W. Park, T. H. Lee, D. G. Park, S. G. Kim, and S. H. Yoon, “Pyrolysis effect of nitrous oxide depending on reaction temperature and residence time,” Journal of the Korean Society of Marine Environment & Safety, vol. 27, no. 7, pp. 1074-1081, 2021.

[22] S. Y. Jin, J. G. Seo, H. J. Kim, S. H. Shin, D. H. Nam, S. M. Kim, D. H. Kim, and S. H. Yoon, “Treatment technology of N_2O by using bunsen premixed flame,” Journal of the Korean Society of Marine Environment & Safety, vol. 27, no. 1, pp. 153-160, 2021.

[23] Y. M. An, D. S. Park, J. G. Nam, and Y. H. Ryu, “Preliminary study of reducing nitrogen oxide emissions according to vanadia precursor of Urea-SCR catalyst in diesel engines,” Journal of the Korean Society of Marine Engineering, vol. 42, no. 9, pp. 697-701, 2018.

[24] S. J. Lee, J. G. Yun, H. M. Lee, J. Y. Kim, J. H. Yun, and J. G. Hong, “Dependence of N_2O/NO decomposition and formation on temperature and residence time in thermal reactor,” Energies, vol. 14, no. 4, p. 1153, 2021.

[25] J. E. Johnsson, P. Glarborg, and K. Dam-Johansen, “Thermal dissociation of nitrous oxide at medium temperatures,” Symposium International on Combustion, vol. 24, no. 1, pp. 917-923, 1992.

[26] M. T. Allen, R. A. Yetter, and F. L. Dryer, “The decomposition of nitrous oxide at $1.5 \leqslant P \leqslant 10.5$ atm and $1103 \leqslant T \leqslant 1173$ K,” International Journal of Chemical Kinetics, vol. 27, no. 9, pp. 883-909, 1995.

[27] R. J. Kee, F. M. Rupley, and J. A. Miller. Chemkin-II: A Fortran Chemical Kinetics Package for the Analysis Of Gas-Phase Chemical Kinetics, SAND-89-8009, Sandia National Lab (SNL-CA), Livermore, CA (United States), 1989.

[28] G. P. Smith, GRI-Mech 3.0. http://www. me. berkley. edu/gri_mech/, 1999.

[29] Y. B. Zel’dovich, “The oxidation of nitrogen in combustion explosions,” Acta Physiochimica U.S.S.R, vol. 21, pp. 577-628, 1946.